

Preparation and characterization of Zr-MCM-41 synthesized under microwave irradiation condition for acetylation of 1,2-dimethoxybenzene with acetic anhydride

K. Bachari · R. Chebout · R. M. Guerroudj · M. Lamouchi

Received: 22 March 2011 / Accepted: 22 July 2011 / Published online: 14 August 2011
© Springer Science+Business Media B.V. 2011

Abstract The liquid phase of acetylation of 1,2-dimethoxybenzene with acetic anhydride has been investigated over a series of acid zirconium mesoporous materials (Zr-MCM-41) synthesized by a microwave irradiation method with different Si/Zr ratios (Si/Zr = 90, 60, 10) and characterized by several spectroscopic techniques such as: N₂ physical adsorption, ICP, XRD, TEM, FT-IR, UV–vis and a temperature-programmed desorption (TPD) of pyridine. In fact, the catalyst Zr-MCM-41 (10) showed a greater performance in the acid-catalyzed acetylation of 1,2-dimethoxybenzene employing acetic anhydride as an acylating agent. Furthermore, the kinetics of the acetylation of 1,2-dimethoxybenzene over these catalysts have also been investigated.

Keywords Zr-MCM-41 materials · 1,2-dimethoxybenzene · Microwave irradiation · Acetylation · Acetic anhydride

Introduction

The microwave–hydrothermal synthesis of molecular sieves is a relatively new area of research [1–7]. It offers many distinct advantages over conventional hydrothermal synthesis. They include rapid heating to crystallization temperature due to volumetric heating, resulting in homogeneous nucleation, fast supersaturation by the rapid dissolution of precipitated gels and eventually a shorter crystallization time compared

K. Bachari (✉) · R. Chebout · R. M. Guerroudj
Centre de Recherche Scientifique et Technique en Analyses Physico-Chimiques (C.R.AP.C),
Alger RP, BP 248, 16004 Alger, Algeria
e-mail: bachari2000@yahoo.fr

M. Lamouchi
Laboratoire de Catalyse et Environnement, EA 2598, MREI, Université du Littoral-Cote d’Opale,
145, Avenue Maurice Schumann, 59140 Dunkerque Cedex, France

to conventional autoclave heating [1–7]. It is also energy efficient and economical [1–7]. On the other hand, Friedel–Crafts acylation of aromatic compounds and aromatic heterocyclic compounds is an excellent example of electrophilic substitution catalyzed by acidic or basic catalysts, which has been widely used in the industry for the production of various organic value-added intermediates. Preparation of aromatic ketones has received much attention in recent years because of their commercial importance, being used as intermediates in the synthesis of pharmaceuticals (naproxen, dextromethorphan, ibuprofen), dyes, fragrances, and agrochemicals [8]. Conventionally, these reactions are carried out in the presence of homogeneous catalysts such as AlCl_3 , and BF_3 , strong mineral acids like H_2SO_4 , HF, or supported Lewis acid catalysts, using acid chloride or anhydride as an acylating agent [9]. Regrettably, the use of the above catalysts in the industry causes a lot of environmental-related problems as they are highly corrosive in nature and cannot be regenerated for further use. Moreover, the separation of the homogeneous catalysts from the product mixture is difficult and often a stoichiometric quantity excess of the catalysts is required as the Lewis acid catalysts form a complex with the product ketones, which is then destroyed in the hydrolysis step required for product isolation. To avoid the above environmental-associated problems, it is desirable to develop a catalyst process which is stable, environmentally friendly, and recyclable. A class of interesting catalytic systems which has been widely used these days and can eliminate the corrosion and environmental problems is the heterogeneous solid Brønsted acid zeolites and zeotypes molecular sieves, which are highly efficient, sustainable, recyclable, and ecofriendly. Indeed, the acetylation of anisole and 1,2-dimethoxybenzene leads to the synthesis of *p*-acetylanisole and 4-acetylveratrole, which are commercially important products and are being used as the precursors of a sun protector and of a component in an insecticide formulation [10], respectively. Different catalysts, including zeolites [11–14], heteropoly acids [15, 16], sulfated metal oxides [17] and AISBA-15 [18], have been investigated for the Friedel–Crafts alkylation and acetylation reactions. Indeed, in the present study, we have studied the liquid phase of acetylation of 1,2-dimethoxybenzene with acetic anhydride over Zr-MCM-41 catalysts synthesized by a microwave irradiation method.

Experimental

Synthesis of the catalysts

Microwave–hydrothermal (M–H) synthesis of Zr-MCM-41 mesoporous molecular sieves with different Si/Zr ratios (Si/Zr = 90, 60, 10) was performed using a MARS5 (CEM, Matthews, NC, USA) microwave digestion system. This system operates at a maximum power of 1,200 W. The power can be varied from 0 to 100%, and is controlled by both pressure and temperature to a maximum of 350 psi and 513 K, respectively. A 2.45-GHz microwave frequency was used which is the same as that in domestic microwave ovens. The syntheses were carried out in double-walled digestion vessels which have an inner liner and cover made up of Teflon PFA and an outer strength vessel shell of Ultem polyetherimide. In a typical

synthesis, 21.32 g of sodium metasilicate ($\text{Na}_2\text{SiO}_3 \cdot 9\text{H}_2\text{O}$, CDH) was dissolved in 60 g of water. The reaction mixture was stirred for 2 h. Meanwhile, cetyltrimethylammonium bromide (5.47 g, CTABr, OTTO Chemie) and zirconium sulfate ($\text{Zr}(\text{SO}_4)_2 \cdot 4\text{H}_2\text{O}$, Merck) were dissolved in 20 g of distilled water. Then, the resultant solution was added dropwise to the sodium metasilicate solution. The final mixture was stirred for 1 h. The pH of the gel was adjusted by using 2 M sulfuric acid (H_2SO_4 ; 98% Merck) and it was stirred for another 3 h. The gel thus obtained was allowed to crystallize under microwave–hydrothermal conditions at 373 K for 2 h. The crystallized product was filtered off, washed with warm distilled water, dried at 383 K and finally calcined at 813 K in air for 6 h.

Characterization techniques

The X-ray diffraction (XRD) patterns of samples were recorded with a powder XRD instrument (Rigaku D/max 2500PC) with Cu $K\alpha$ radiation ($\lambda = 0.15418$ nm). It was operated at 40 kV and 50 mA. The experimental conditions correspond to a step width of 0.02° and a scan speed of $1^\circ/\text{min}$. The diffraction patterns were recorded in the 2θ range of $1\text{--}10^\circ$. Fourier transform infrared spectra of samples were recorded on a Nexus FT-IR 470 spectrometer made by Nicolet (USA) with the KBr pellet technique. The effective range was from 400 to $4,000\text{ cm}^{-1}$. Specific surface area and pore size were measured by using a NOVA2000e analytical system made by Quantachrome (USA). The specific surface area was calculated by the Brunauer–Emmett–Teller (BET) method. Pore size distribution and pore volume were calculated by the Barrett–Joyner–Halenda (BJH) method. Transmission electron microscopy (TEM) morphologies of samples were observed on a Philips TEMCNAI-12 with an acceleration voltage of 100–120 kV. Diffuse reflectance UV–Vis spectra were recorded on a UV-3100 spectrophotometer made by Shimadzu (Japan) with spherical diffuse reflectance accessory, using BaSO_4 as a reference. The zirconium content in the samples was determined by inductively coupled plasma (ICP) technique (Vista-MAX, Varian). The density and strength of the acid sites of the different Zr-MCM-41 samples were determined by the temperature-programmed desorption (TPD) of pyridine. About 100 mg of the materials were evacuated for 3 h at 523 K under vacuum ($P < 10^{-5}$ kPa). Thereafter, the samples were cooled to room temperature under dry nitrogen followed by exposure to a stream of pyridine in nitrogen for 30 min. Subsequently, the physisorbed pyridine was removed by heating the sample to 393 K for 2 h in a nitrogen flow. The temperature-programmed desorption (TPD) of pyridine was performed by heating the sample in a nitrogen flow (50 mL/min) from 393 to 873 K with a rate of 10 K/min using a high-resolution thermogravimetric analyzer coupled with a mass spectrometer (SETARAM setsys 16MS). The observed weight loss was used to quantify the number of acid sites assuming that each mole of pyridine corresponds to one mole of protons.

Catalytic testing

Acetylation of 1,2-dimethoxybenzene with acetyl chloride was carried out under liquid phase conditions. The liquid phase reaction set up consists of two-necked

50-mL round bottom flask duly fitted with a condenser in one end for cooling while the other vent is closed with a Teflon septum for collecting samples by glass syringe at regular intervals. The whole system was kept in a thermostated oil bath with a magnetic stirrer coupled to a heating plate. In a typical reaction, the catalyst was added to a solution of 2.6 g 1,2-dimethoxybenzene (18.9 mmol), 0.4 g acetyl chloride (3.8 mmol) and 50 mL chlorobenzene together with 1 g nitrobenzene as internal standard. Then, the reaction mixture was heated to the required temperature and the samples were collected at regular time intervals. The collected samples were analyzed periodically by a gas chromatograph (HP-6890) equipped with a FID detector using a DB-5 capillary column. The products were confirmed with GC-MS (HP-5973) analysis.

Results

Characterization of the samples

The small angle X-ray diffraction patterns of Zr-MCM-41 (Si/Zr = 90, 60, 10) synthesized by the microwave irradiation method are shown in Fig. 1. The Zr-MCM-41 (90) sample gives a very strong (100) peak followed by (110) and (200) lower intensity peaks. All three distinct Bragg reflections at low angles were

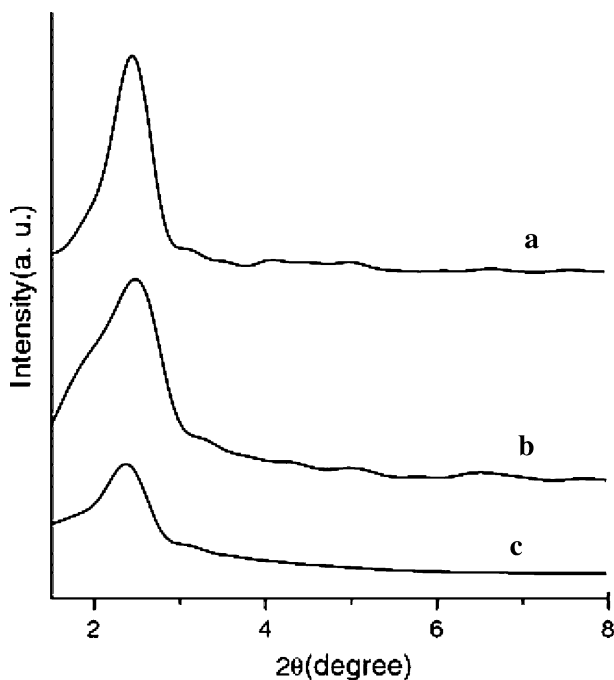


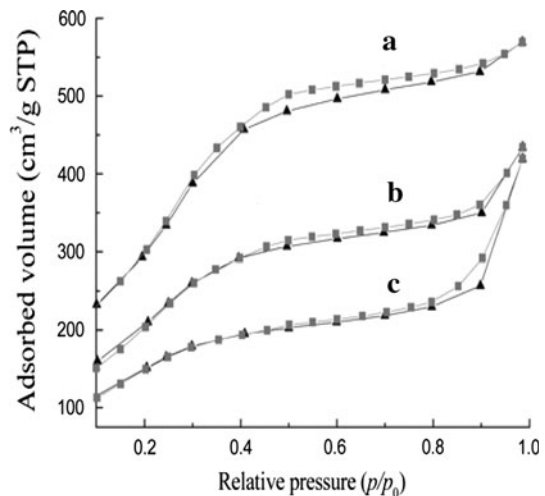
Fig. 1 XRD patterns of Zr-MCM-41 materials in the domain of $1\text{--}10^\circ$ (2θ) prepared by microwave-hydrothermal (M-H) process: *a* Zr-MCM-41 (90), *b* Zr-MCM-41(60), *c* Zr-MCM-41(10)

indexed on the hexagonal lattice. However, when the zirconium content ratio increased from 60 to 10, the intensities of the long-range ordered peaks were gradually reduced. However, compared with the pattern of the typical MCM-41 mesoporous molecular sieve [19], it can be noted that the d_{100} spacing in Zr-MCM-41 samples is significantly larger than MCM-41 (for both as-synthesized and calcined samples) and shows the incorporation of Zr in the MCM-41 structure. The zirconium content in Zr-MCM-41 is increased with Zr content in the synthesis gel (Table 1). The porosity of the samples was evaluated by N_2 adsorption isotherms. Figure 2 shows the N_2 adsorption–desorption isotherms of the three calcined samples of Zr-MCM-41. The specific surface areas and pore size distributions and pore volumes calculated by the BET and BJH methods are summarized in Table 1. According to Fig. 2, the N_2 adsorption–desorption isotherms of the two samples Zr-MCM-41(90) and Zr-MCM-41(60) exhibit typical type IV isotherms with hysteresis loop caused by capillary condensation in mesopores, manifesting that the two samples possess the obvious mesoporous structure [19]. There are three well-defined stages in the isotherms of the two samples that may be identified. The isotherms show a step at the relative pressure (p/p_0) of ca. 0.3–0.4, characteristic of capillary condensation of uniform mesoporous materials, showing that the two samples have uniform pore size distribution and larger pore volume. The isotherms corresponding to $p/p_0 < 0.3$ are due to a monolayer adsorption of nitrogen on the

Table 1 Physicochemical properties of different Zr-MCM-41 (M–H) samples

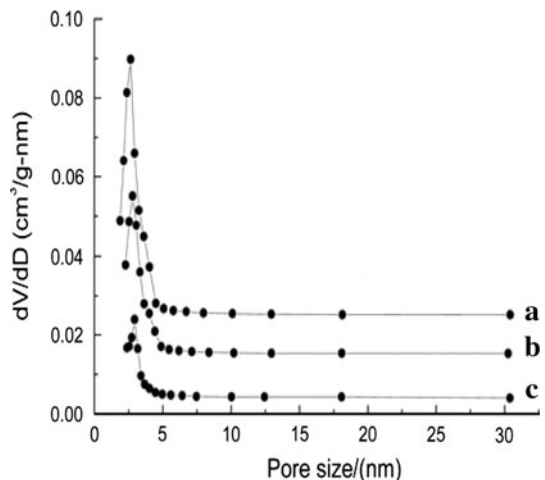
Sample	Chemical analysis		S_{BET} , $\text{m}^2 \text{g}^{-1}$	Pore volume, $\text{cm}^3 \text{g}^{-1}$	Pore diameter, nm
	Si/Zr (gel)	Si/Zr			
Zr-MCM-41	10	10.7	686	0.66	2.9
Zr-MCM-41	60	59.5	918	0.88	2.7
Zr-MCM-41	90	92.4	1150	0.98	2.6

Fig. 2 N_2 physical adsorption–desorption isotherms of Zr-MCM-41 materials prepared by microwave–hydrothermal (M–H) process: *a* Zr-MCM-41 (90), *b* Zr-MCM-41(60), *c* Zr-MCM-41(10)



walls of the mesopore. The near-horizontal section beyond $p/p_0 > 0.4$ represents the multilayer adsorption on the outer surface of the particles. In addition, from Fig. 2, we can observe that the isotherms of the sample Zr-MCM-41(90) have a sharper capillary condensation step at the same p/p_0 , illustrating that it possesses more uniform pore size distribution as compared with the isotherms of the other sample. Moreover, the isotherms of the sample Zr-MCM-41(10) did not fit into typical type IV isotherms; this is attributed to the partial damage of the mesoporous structure caused by the overfull zirconium ions incorporated into the MCM-41 mesoporous molecular sieve. However, combined with the surface area data ($686 \text{ m}^2/\text{g}$) listed in Table 1 and the XRD data (Fig. 1), the sample Zr-MCM-41(10) still has a partial mesoporous structure, but the ordering is poor. Figure 3 presents the pore size distribution curves of the three calcined samples Zr-MCM-41 synthesized by the microwave irradiation method. As shown in Fig. 3, narrow and sharp peaks can be observed in a pore size range of ca. 2–3 nm for the samples Zr-MCM-41(90) and Zr-MCM-41(60), and the intensity of the peak is also strong as compared with that of the sample Zr-MCM-41(10), indicating that the two samples also have uniform pore size distribution. Additionally, as the zirconium content in the sample increased, the intensity of the pore size distribution peak became weak, which reflects that the increase of zirconium ions incorporated into the silica framework of MCM-41 mesoporous molecular sieve caused the partial distortion of the mesoporous framework, resulting in the irregular pore size distribution and the poor mesoporous ordering. From Table 1, we can conclude that the specific surface area and pore volume of the resulting samples gradually decreased as the zirconium content increased, and that the pore size is in the range of 2.5–2.9 nm. Combined with the results of XRD and N_2 adsorption isotherms, it is reasonable to conclude that the mesoporous ordering of the sample Zr-MCM-41 synthesized by the microwave irradiation method gradually decreased with the increase of the zirconium content incorporated into the mesoporous framework. Figure 4 presents the FT-IR spectra of the synthesized Zr-MCM-41(60) sample before and after

Fig. 3 Pore size distribution curves of the of Zr-MCM-41 materials prepared by the microwave–hydrothermal (M–H) process: *a* Zr-MCM-41(90), *b* Zr-MCM-41(60), *c* Zr-MCM-41(10)



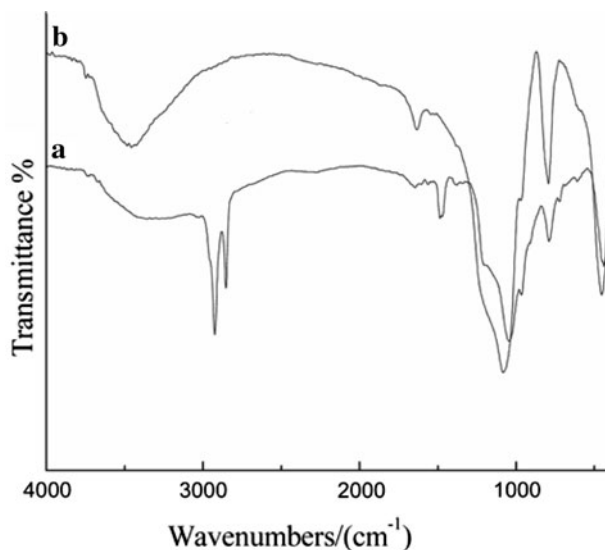


Fig. 4 FT-IR spectra of the Zr-MCM-41(60) material prepared by the microwave-hydrothermal (M-H) process: *a* before calcination and *b* after calcinations

calcination at 813 K in air for 6 h. As shown in Fig. 4, the band at $3,500\text{ cm}^{-1}$ is the characteristic band of the water adsorbed on the sample surface. The bands at $1,620\text{--}1,640\text{ cm}^{-1}$ are aroused by the flexion vibration of the OH bond [20]. The band at $1,080\text{ cm}^{-1}$ is from the asymmetric extension vibration of Si-O-Si. The band about 810 cm^{-1} is due to the corresponding symmetric vibration of the Si-O-Si bond, while the band at 460 cm^{-1} is assigned to rocking vibration of the Si-O-Si bond. The bands at $2,921$, $2,850$ and $1,480\text{ cm}^{-1}$ are the characteristic bands of the surfactant alkyl chains. After the sample Zr-MCM-41(60) was calcined at 813 K in air for 6 h, the bands at $2,921$, $2,850$ and $1,480\text{ cm}^{-1}$ disappeared, certifying that the template had been effectively removed. The diffuse reflectance UV-vis spectra of the three samples Zr-MCM-41 are presented in Fig. 5. As shown in Fig. 5, it can be observed that the samples Zr-MCM-41 all show one single peak at ca. 205–220 nm and the intensity also increases with the increase in the Zr content of the samples. Generally, the position of the adsorption peak associated with ligand to metal charge transfer ($\text{O}^{2-} \rightarrow \text{Zr}^{4+}$) spectra depends on the ligand field symmetry surrounding the zirconium center. And the electronic transitions from oxygen to tetra-coordinated Zr^{4+} require a higher energy as compared with hexa-coordinated one. Therefore, it may be suggested that the adsorption peak at ca. 205–220 nm for the samples Zr-MCM-41 is probably attributed to the presence of one type of zirconium species-tetra-coordinated Zr^{4+} . It is probably that the Zr (IV) species has been incorporated into the framework of the sample MCM-41 [21]. The TEM images of the samples Zr-MCM-41(90), Zr-MCM-41(60) and Zr-MCM-41(10) are shown in Fig. 6. It can be observed that two samples exhibited the hexagonal arrays structure, indicating that the three samples synthesized under microwave irradiation condition possess the mesoporous framework. However, the mesoporous ordering

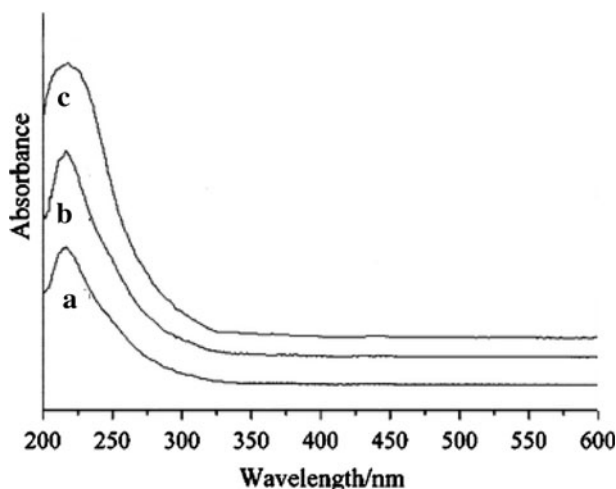


Fig. 5 Diffuse reflectance UV-vis spectra of the samples Zr-MCM-41 prepared by the microwave-hydrothermal (M-H) process: *a* Zr-MCM-41 (90), *b* Zr-MCM-41(60), *c* Zr-MCM-41(10)

of the sample Zr-MCM-41(10) is poor as compared to that of the samples Zr-MCM-41 (60) and Zr-MCM-41 (90). Additionally, it can also be observed that there are no particles and/or clusters containing zirconium species on the surface of the three samples in Fig. 6. Furthermore, the acid site distribution and acid amounts of Zr-MCM-41 synthesized under the microwave irradiation condition were determined using temperature-programmed desorption (TPD) of pyridine; the data are presented in Table 2. Weak (423 and 633 K), moderate (633–743 K) and strong (>743 K) acid sites are found in all samples. The weak acid sites are attributed to surface hydroxyl groups and the medium and the strong acid sites probably originate from the incorporation of zirconium atoms into the MCM-41 walls. It is interesting to note that the number of weak acids sites decreases with decreasing Si/Zr ratio. However, the amount of medium and strong acid sites decreases with increasing Si/Zr ratio. It should be noted that the total number of acid sites (medium and strong acid sites) of Zr-MCM-41 (10) prepared by the microwave-hydrothermal (M-H) process is higher than that of Zr-MCM-41 (60) and Zr-MCM-41 (90).

Catalytic activity

Catalytic performances of Zr-MCM-41(M-H) materials with different Si/Zr ratio in the acetylation of 1,2-dimethoxybenzene with acetic anhydride

The acetylation of 1,2-dimethoxybenzene has been carried out over Zr-MCM-41 (M-H) materials with different Zr contents (Si/Zr = 90, 60, and 10) using acetic anhydride as an acylating agent. The acetylation of 1,2-dimethoxybenzene with acetic anhydride generates acetic acid in the products, which resulted from the acetic anhydride utilization. Only one product is obtained, which is 3,4-dimethoxyacetophenone, due to the fact that both the ortho positions of

Fig. 6 TEM images of the Zr-MCM-41(90), Zr-MCM-41(60) and Zr-MCM-41(10) materials prepared by the microwave-hydrothermal (M-H) process

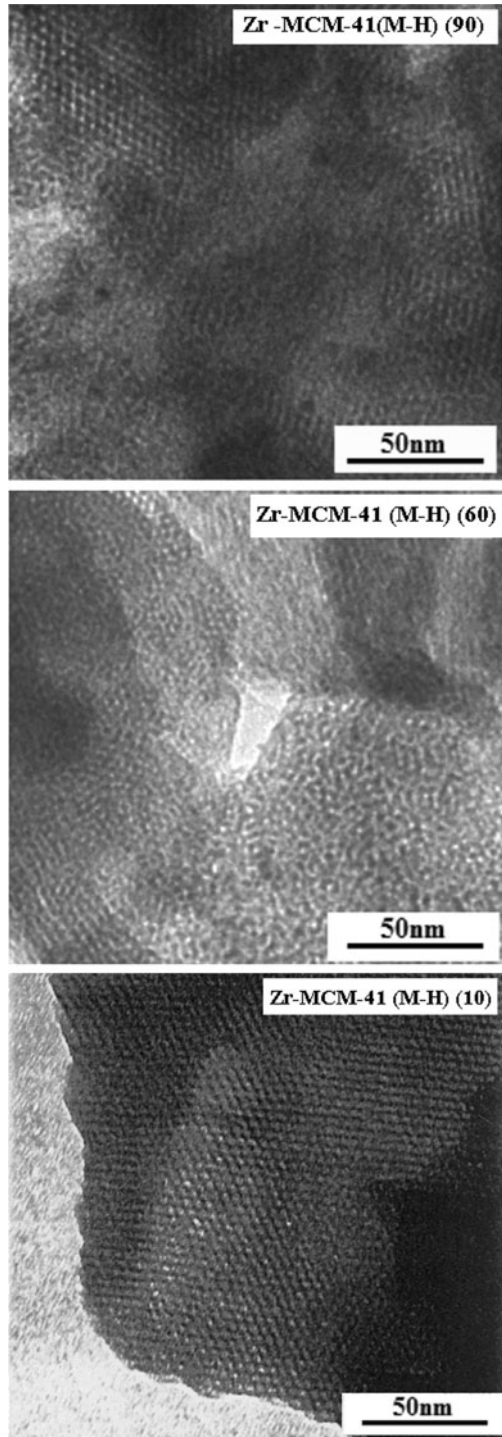


Table 2 Density and strength of acid sites of Zr-MCM-41 (M–H) catalysts with different Si/Zr ratios (Si/Zr = 90, 60, 10)

Sample	Acid sites (mmol/g)			
	Weak (423–633 K)	Medium (633–743)	Strong (>743)	Total (medium and strong acid sites)
Zr-MCM-41 (10)	0.539	0.191	0.224	0.415
Zr-MCM-41 (60)	0.601	0.123	0.179	0.302
Zr-MCM-41 (90)	0.748	0.107	0.145	0.252

1,2-dimethoxybenzene are sterically crowded for electrophilic reaction; acetylation preferentially occurs at the fourth position which is the most favored and para to one of the methoxy substituents. No products other than 3,4-dimethoxyacetophenone were found in the product mixture. The conversion and the selectivity in the acetylation of 1,2-dimethoxybenzene over Zr-MCM-41 (M–H) catalysts with different Si/Zr ratio (Si/Zr = 90, 60, and 10) at a reaction temperature of 333 K and under the standard reaction conditions (stoichiometric ratio 1,2DMB/AC = 5, catalyst weight = 0.1 g and a reaction time of 2 h) are given in Table 3. The activity of the catalysts is in the following order: Zr-MCM-41 (M–H) (10) > Zr-MCM-41 (M–H) (60) > Zr-MCM-41 (90). In fact, it is found that Zr-MCM-41(10) is the mainly efficient catalyst, show much higher conversion of acetic anhydride as compared with that of other catalysts studied. The Zr-MCM-41(10) catalyst registers the complete acetic anhydride conversion and 100% selectivity to 3,4-dimethoxyacetophenone after 95 min of reaction. The very higher activity of Zr-MCM-41(10) than other Zr-MCM-41 (M–H) catalysts may be mostly attributed by the fact that the catalyst exhibits higher acidity than other Zr-MCM-41 (M–H) catalysts (Table 2). On the other hand, the lower activity of Zr-MCM-41 (M–H) (90) which has the highest surface area and larger pore volume is mainly due the presence of lower number of active sites on the porous surface. Elsewhere, it was interesting to compare the solids with zeolites catalysts investigated earlier under similar conditions. The activity of the catalysts is in the following order: Zr-MCM-41(M–H) (10) > BEA > MFI. Indeed, it must be noted that, although the acidity of the zeolites catalysts is much higher than that of the Zr-MCM-41 (M–H) (10), the catalytic activity of the later is superior to that of zeolites catalysts. Thus, it has to be

Table 3 The conversion and the selectivity of 1,2-dimethoxybenzene over Zr-MCM-41 (M–H) catalysts with different Si/Zr ratio (Si/Zr = 90, 60, and 10) at a reaction temperature of 333 K, stoichiometric ratio 1,2DMB/AC = 5, catalyst weight = 0.1 g and a reaction time of 2 h

Sample	Acetic anhydride conversion (%)	Selectivity to 3, 4-dimethoxyacetophenone (%)
Zr-MCM-41 (M–H) (10)	100.0	100.0
Zr-MCM-41 (M–H) (60)	88.3	100.0
Zr-MCM-41 (M–H) (90)	66.5	100.0

concluded that the accessibility of the active sites by the reactant molecules is higher in Zr-MCM-41 (M–H) (10) than that of the zeolite catalysts, which is supported by their enormous specific surface area and the specific pore volume, and large pore diameter with well-ordered pore structure. These exceptional textural characteristics of the Zr-MCM-41 (M–H) (10) are accountable for its higher catalytic activity and the results further confirm that the catalysts with high surface area, and large pore diameter is highly important for acetylation of substituted aromatic compounds. As the Zr-MCM-41 (M–H) (10) catalyst was found to be highly active, we opted to choose the catalyst for investigating the effect of other reaction parameters such as the reaction temperature, the stoichiometric ratio 1,2DMB/AC, weight of the catalysts and the recycling of the catalysts on the conversion of acetic anhydride and the selectivity in the acetylation of 1,2-dimethoxybenzene.

The effect of reaction temperature in the acetylation of 1,2-dimethoxybenzene with acetic anhydride

The effect of reaction temperature on the conversion of acetic anhydride in the acetylation of 1,2-dimethoxybenzene over Zr-MCM-41 (M–H) (10) at different reaction times is shown in Table 4. As expected, an increase in the reaction temperature had a favorable effect on the conversion of the acetic anhydride. The conversion of acetic anhydride increases with increasing the reaction temperature. However, the selectivity to 3,4-dimethoxyacetophenone was not changed with increasing the reaction temperature. The selectivity of the product was almost 100% for all the reaction temperature studied. It must be noted that the rate of the reaction at lower temperature is rather slow. On the other hand, at the reaction temperature more than 333 K, the rate of the reaction is very fast. The apparent rate constant of the reaction at different reaction temperature was calculated using the pseudo-first order rate law:

$$\text{Log} [1/1 - x] = (k_a/2.303)(t - t_0)$$

where k_a is the apparent first-order rate constant, x the fractional conversion of acetic anhydride, t the reaction time and t_0 the induction period corresponding to the time required for reaching equilibrium temperature. A plot of $\log [1/1 - x]$ as a function of the time gives a linear plot over a large range of acetic anhydride conversions. As expected, the apparent rate constant for the acetylation reaction was

Table 4 Catalytic activities of Zr-MCM-41 (M–H) (10) at different temperatures: 313, 333 and 353 K, stoichiometric ratio 1,2DMB/AC = 5, catalyst weight = 0.1 g

Temperature (K)	Time ^a (min)	Selectivity to 3,4-dimethoxyacetophenone (%)	Apparent rate constant k_a ($\times 10^3 \text{ min}^{-1}$)
313	210.2	100.0	13.2
333	95.0	100.0	40.3
353	40.1	100.0	94.4

^a Time required for complete conversion of acetic anhydride

increased from $13.2 \cdot 10^{-3}$ to $94.4 \cdot 10^{-3} \text{ min}^{-1}$ with increasing the reaction temperature from 313 to 363 K. The activation energy for the Zr-MCM-41(10) calculated from an Arrhenius plot, was found to be 28.2 kJ mol^{-1} . From these results, it is found that the reaction temperature of 333 K is the best temperature for Zr-MCM-41(10) and is preferred for the subsequently catalytic studies.

The effect of the stoichiometric ratio 1,2DMB/AC on the acetylation of 1,2-dimethoxybenzene with acetic anhydride

The effect of the stoichiometric ratio 1,2DMB/AC on the conversion of acetic anhydride was studied over Zr-MCM-41 (M–H) (10) at a reaction temperature of 333 K as a function of reaction time and the results are shown in Table 5. When the 1,2DMB/AC ratio was varied, the conversion of acetic anhydride was significantly affected. The conversion of acetic anhydride is increased by increasing the 1,2DMB/AC from 1 to 10 at a reaction temperature of 333 K, while the selectivity to 3,4-dimethoxyacetophenone is almost constant in all the cases. It was found that the increase of the 1,2DMB/AC ratio may support the adsorption of a greater amount of 1,2-dimethoxybenzene on the catalysts surface compared to acetic anhydride molecules.

The effect of the weight of the catalysts in the acetylation of 1,2-dimethoxybenzene with acetic anhydride

The weight of the catalysts was varied to study its influence on the conversion of acetic anhydride in the acetylation of 1,2-dimethoxybenzene over Zr-MCM-41 (M–H) (10). The weight of the catalysts in the reaction mixture was changed from 0.02 to 0.2 g. Table 6 shows the influence of the weight of the Zr-MCM-41 (M–H) (10) catalyst on the conversion of the acetic anhydride in the acetylation of 1,2-dimethoxybenzene. The concentration of the catalyst in the reaction mixture has a huge impact on the conversion of acetic anhydride. The conversion of the acetic anhydride increases when increasing the weight of the catalyst from 0.02 to 0.2 g at the reaction temperature of 333 K and the stoichiometric ratio 1,2DMB/AC = 5, whereas maintaining 100% selectivity to 3,4-dimethoxyacetophenone. This could be mostly due to the fact that the accessibility of the surface acidic sites is larger at

Table 5 The conversion and the selectivity in the acetylation of 1,2-dimethoxybenzene over Zr-MCM-41 (M–H) (10) catalyst with different stoichiometric ratio 1,2DMB/AC at a reaction temperature of 333 K, catalyst weight = 0.1 g

Stoichiometric ratio 1,2DMB/AC	Time ^a (min)	Selectivity to 3,4-dimethoxyacetophenone (%)	Apparent rate constant k_a ($\times 10^3 \text{ min}^{-1}$)
1	255.3	100.0	10.1
5	95.0	100.0	40.3
10	64.3	100.0	70.2

^a Time required for complete conversion of acetic anhydride

Table 6 The conversion and the selectivity in the acetylation of 1,2-dimethoxybenzene over Zr-MCM-41 (M–H) (10) catalyst with different weight of the catalyst at a reaction temperature of 333 K, stoichiometric ratio 1,2DMB/AC = 5

Weight of the catalyst (g)	Time ^a (min)	Selectivity to 3,4-dimethoxyacetophenone (%)	Apparent rate constant k_a ($\times 10^3 \text{ min}^{-1}$)
0.02	289.5	100.0	8.9
0.1	95.0	100.0	40.3
0.2	58.9	100.0	79.8

^a Time required for complete conversion of acetic anhydride

higher catalyst concentrations, which supports the increase in the conversion of acetic anhydride.

Recycling of the catalysts

The recyclability has been done over Zr-MCM-41 (M–H) (10) in the acetylation of 1,2-dimethoxybenzene at a reaction temperature of 333 K, a reaction time of 2 h, and a 1,2DMB/AC ratio of 5. After the reaction, the catalyst was filtered, washed several times with acetone and dried in an oven at 393 K. Then, the catalyst was activated at 823 K for 6 h under oxygen atmosphere. The recyclability experiments were carried out twice and the procedure for the activation was repeated every time after the reaction. The results on the recyclability are given in Table 7. The catalyst shows approximately similar conversion after two cycles, without any transformation in the selectivity of the products. This shows that the catalyst is very stable under the specified reaction conditions, and able to be recycled.

Applications to other aromatic compounds

The acetylation of other substrates with acetic anhydride was accomplished using Zr-MCM-41(10) under the optimized reaction conditions. The information concerning the reaction conditions and the results are presented in Table 8. The catalyst shows amazing performances in the acetylation of aromatics used in the reaction. In the case of acetylation of méthoxybenzène (anisole), it was observed that the time required for complete conversion of acetic anhydride over Zr-MCM-41

Table 7 Effect of recycling the catalyst in the acetylation of 1,2-dimethoxybenzene over Zr-MCM-41 (M–H) (10) at a reaction temperature of 333 K, stoichiometric ratio 1,2DMB/AC = 5, catalyst weight = 0.1 g

Catalyst	Time ^a (min)	Selectivity to 3,4-dimethoxyacetophenone (%)	Apparent rate constant k_a ($\times 10^3 \text{ min}^{-1}$)
Fresh	95.0	100.0	40.3
First reuse	99.2	100.0	37.6
Second reuse	102.5	100.0	33.9

^a Time required for complete conversion of acetic anhydride

Table 8 Acetylation of different aromatic substrates over Zr-MCM-41 (M–H) (10) catalyst at a reaction temperature of 333 K

Substituent	Time ^a (min)	Reaction products (Selectivity (%))
1,2-dimethoxybenzene	95	3,4-dimethoxyacetophenone (100%)
Methoxybenzene (anisole)	27	<i>p</i> -methoxyacetophenone (98.5%) <i>o</i> -methoxyacetophenone (1.5%)
2-Methoxy naphthalene	37	1-acetyl-2-methoxynaphthalene (97.4%) 6-acetyl-2-methoxynaphthalene (2.6%)

^a Time required for complete conversion of acetic anhydride

(M–H) (10) catalyst is 27 min with 98.5% selectivity to (*p*) 4-methoxyacetophenone, while the rest is (*o*) 2-methoxyacetophenone. The data on the acetylation of 2-methoxynaphthalene with acetic anhydride under nitrobenzene as solvent are also presented in Table 8. In fact, the selectivity to 1-acetyl-2-methoxynaphthalene and 6-acetyl-2-methoxynaphthalene of 97.4 and 2.6%, respectively, was observed. The formation of the sterically hindered, but kinetically favored, product, 1-acetyl-2-methoxynaphthalene, has also been observed for the zeolite catalysts with greater external surface areas and the proton exchanged MCM-41 catalyst at low reaction temperature because the position 1 is considered to be the most activated one [22, 23]. Therefore, we consider the preferential formation of 1-acetyl-2-methoxynaphthalene in the Zr-MCM-41 (M–H) catalysts system could be mostly due the fact that the materials possess large surface area, pore volume and pore diameter which support the formation of the kinetically favored 1-acetyl-2-methoxynaphthalene rather than the thermodynamically favored 6-acetyl-2-methoxynaphthalene.

Conclusion

Ordered hexagonal Zr-MCM-41 mesoporous molecular sieves with high specific surface area were successfully synthesized via the microwave irradiation method. After the calcination, the template was effectively removed. The Si/Zr molar ratio is a key factor influencing the textural properties and structural regularity of Zr-MCM-41 mesoporous molecular sieves. High zirconium content is unfavorable to the formation of the Zr-MCM-41 with a highly ordered mesoporous structure. These samples have many medium acid sites. The study of the liquid phase of acetylation of 1,2-dimethoxybenzene and other two aromatic compounds with acetic anhydride using Zr-MCM-41 solids shows that these catalysts have remarkable activities and can also be reused in this reactions for several times.

References

1. S.C. Laha, G. Kamalakar, R. Glaser, *Microporous Mesoporous Mater.* **90**, 45 (2006)
2. K. Bachari, M. Lamouchi, *J. Clust. Sci.* **20**, 573 (2009)

3. S.H. Jhung, J.-S. Chang, J.S. Hwang, S.-E. Park, *Microporous Mesoporous Mater.* **64**, 33 (2003)
4. K. Bachari, R.M. Guerroudj, M. Lamouchi, *React. Kinet. Mech. Catal.* **102**, 219 (2011)
5. G. Tompsett, W.C. Conner, K.S. Yngvesson, *Chem. Phys. Chem.* **7**, 296 (2006)
6. S.-E. Park, J.-S. Chang, Y.K. Hwang, D.S. Kim, S.H. Jhung, J.-S. Hwang, *Catal. Surv. Asia* **8**, 91 (2004)
7. K. Bachari, M. Lamouchi, *Trans. Metal Chem.* **34**, 529 (2009)
8. G. Franck, J.W. Stadelhofer, *Industrial Aromatic Chemistry* (Springer, Berlin, 1998)
9. P.H. Gore, in *Friedel Crafts and Related Reactions*, vol. III, ed. by G.A. Olah (Wiley Interscience, New York, 1964), p. 72
10. M. Guidotti, C. Canaff, J.M. Coustard, P. Magnoux, M. Guisnet, *J. Catal.* **230**, 375 (2005)
11. B. Bachiller-Baeza, J.A. Anderson, *J. Catal.* **228**, 225 (2004)
12. V. Quaschnig, J. Deutsch, P. Druska, H.J. Lieske, *J. Catal.* **231**, 269 (2005)
13. E.G. Derouane, G. Crehan, C.J. Dillon, D. Bethell, H. He, S.B. Derouane, A.B.D. Hamid, *J. Catal.* **194**, 410 (2000)
14. T. Raja, A.P. Singh, A.V. Ramaswamy, A. Finiels, P. Moreau, *Appl. Catal.* **211**, 31 (2001)
15. J. Kaur, K. Griffin, B. Harrison, I.V. Kozhevnikov, *J. Catal.* **208**, 448 (2002)
16. I.V. Kozhevnikov, *Appl. Catal. A: Gen.* **256**, 3 (2003)
17. A.M. Cardoso, W. Alves Jr., A.R.E. Gonzaga, L.M.G. Augiar, H.M.C. Andrade, *J. Mol. Catal. A.* **209**, 189 (2004)
18. A. Vinu, J. Justus, C. Anand, D.P. Sawant, K. Ariga, T. Mori, P. Srinivasu, V.V. Balasubramanian, S. Velmathi, S. Alam, *Microporous Mesoporous Mater.* **116**, 108 (2008)
19. J.S. Beck, J.C. Vartuli, W.J. Roth, M.E. Leonowicz, C.T. Kresge, K.D. Schmitt, C.T.-W. Chu, D.H. Olson, E.W. Sheppard, S.B. McCullen, J.B. Higgins, J.L. Schlenker, *J. Am. Chem. Soc.* **114**, 10834 (1992)
20. L.F. Chen, L.E. Noreña, J. Navarrete, J.A. Wang, *Mater. Chem. Phys.* **97**, 236 (2006)
21. Y. Du, Y. Sun, Y. Di, L. Zhao, S. Liu, F.-S. Xiao, *J. Porous. Mater.* **13**, 163 (2006)
22. M.L. Kantam, K.V.S. Ranganath, M. Sateesh, K.B.S. Kumar, B.M. Choudary, *J. Mol. Catal. A: Chem.* **225**, 15 (2005)
23. P. Andy, J. Garcia-Martinex, G. Lee, H. Gonzalez, C.W. Jones, M.E. Davis, *J. Catal.* **192**, 215 (2000)